

# Enantiopreferential DNA Binding of $[\text{Ru}^{\text{II}}(1,10\text{-phenanthroline})_3]^{2+}$ Studied with Linear and Circular Dichroism

Catharina Hiort,<sup>†</sup> Bengt Nordén,<sup>\*†</sup> and Alison Rodger<sup>‡</sup>

Contribution from the Department of Physical Chemistry, Chalmers University of Technology, S-412 96 Gothenburg, Sweden, and the Physical Chemistry Laboratory, South Parks Road, Oxford OX1 3QZ, England. Received March 29, 1989

**Abstract:** Circular dichroism (CD) spectroscopy and linear dichroism (LD) spectroscopy have been used to probe the binding of  $[\text{Ru}^{\text{II}}(1,10\text{-phenanthroline})_3]^{2+}$  to DNA. Changes in CD and normal absorption upon binding and the LD observed in flow-oriented DNA systems are analyzed to yield information about the binding of the  $\Delta$  and  $\Lambda$  enantiomers. Flow LD shows that both isomers bind to DNA but with different geometries. These two types of binding geometries are observed with DNA and  $[\text{poly}(\text{dA-dT})]_2$  in a wide range of binding ratios ( $r = 0.005\text{--}0.1$  metal/DNA phosphate) and ionic strengths, and also with  $[\text{poly}(\text{dG-dC})]_2$ , indicating that the enantiomerically specific geometry is determined by the "texture" (helical pitch and sense) of the double helix, irrespective of base composition. The  $\Lambda$  enantiomer of  $[\text{Ru}^{\text{II}}(1,10\text{-phenanthroline})_3]^{2+}$  shows a pronounced binding affinity for  $[\text{poly}(\text{dA-dT})]_2$  at low binding ratios; however, other combinations of the two enantiomers with this polynucleotide,  $[\text{poly}(\text{dG-dC})]_2$ , and DNA show binding affinities that vary depending on the binding ratio, ionic strength, and concentration of the opposite enantiomer. The binding of the  $\Delta$  enantiomer strongly affects the DNA orientation, indicating a reduced persistence length. In contrast, the  $\Lambda$  enantiomer does not markedly affect the DNA orientation, despite the similar binding types and electronic perturbations indicated by the spectroscopic data for both enantiomers. An earlier speculation that the  $\Delta$  enantiomer should bind with one of its phenanthroline wings partially intercalated between base pairs is inconsistent with an angle of approximately  $70^\circ$  between the 3-fold axis of the complex and the DNA helix axis as concluded from the LD spectra. Both enantiomers are believed to be accommodated in the major groove, but with somewhat different geometries owing to steric interactions. The spectroscopic data are interpreted by using the results from a perturbation theory analysis.

Numerous studies of DNA interactions with chiral tris-chelate metal complexes,  $\text{ML}_3$ , have been inspired by the possibility of discriminating DNA handedness.  $\text{ML}_3$  complexes are shaped like three-bladed propellers and have two enantiomeric forms [corresponding to right- ( $\Delta$ ) and left- ( $\Lambda$ ) handed screws; cf Figure 1] that might be expected to interact differently with helical DNA. It was early observed that the  $\Delta$  enantiomer of  $[\text{Fe}^{\text{II}}(\text{bpy})_3]^{2+}$  (bpy = 2,2'-bipyridyl) exhibits a preferential binding to DNA.<sup>1</sup> The  $\Delta$  enantiomer is also the one preferred by DNA for a number of analogous complexes, such as  $[\text{Zn}^{\text{II}}(\text{phen})_3]^{2+}$ ,<sup>2</sup>  $[\text{Ru}^{\text{II}}(\text{phen})_3]^{2+}$ ,<sup>3-10</sup>  $[\text{Ru}^{\text{II}}(\text{bpy})_3]^{2+}$ ,<sup>11</sup> and  $[\text{Fe}^{\text{II}}(\text{phen})_3]^{2+}$ .<sup>9,11</sup> (phen = 1,10-phenanthroline). For all of these complexes the binding is weak and the chiral discrimination is relatively small, though sufficiently strong for circular dichroism (CD) to show a shift in the diastereomeric equilibria of inversion-labile complexes such as those with iron(II).<sup>1,11</sup>

An enhancement of stereoselectivity has been reported with one complex,  $[\text{Ru}^{\text{II}}(4,7\text{-diphenylphen})_3]^{2+}$ , which is presumably due to the steric effects of the phenyl "wings" of the chelates.<sup>6,12,13</sup> However, the question of whether tris-chelate metal complexes discriminate between B and Z forms of DNA is still controversial,<sup>9</sup> and the details of the DNA/complex interaction are far from well understood.

DNA has a number of types of sites in which a molecule might bind: (i) between two base pairs (full intercalation), (ii) in the minor groove, (iii) in the major groove, and (iv) on the outside of the helix. It has been proposed that the  $\text{ML}_3$  complexes bind in the major groove of DNA.<sup>1-7,12,13</sup> This proposal is supported by the fact that the size of the  $\text{ML}_3$  complex (approximately 10 Å across) precludes it from adopting a fully intercalated site and also suggests that the minor groove would be unfavorable. In addition, the observation of a distinct and quite large LD for several complexes<sup>8,10,11</sup> indicates that external binding sites, which can be anticipated to give poor orientation, are not the only type of site occupied. Fluorescence and electrophoretic mobility measurements on the enantiomers and on racemic mixtures have been used to support a postulate that one of the chelate wings be partially intercalated.<sup>2,4-6</sup> As we shall see, however, this is not

the only possible interpretation of these results.

In this study we have examined the enantioselectivity, and also the binding geometries, of complexes between the inversion-stable  $[\text{Ru}^{\text{II}}(\text{phen})_3]^{2+}$  and DNA,  $[\text{poly}(\text{dA-dT})]_2$ , and  $[\text{poly}(\text{dG-dC})]_2$ , using linear and circular dichroism techniques. We have focused on the electric-dipole-allowed charge-transfer (CT) transitions in the 400-nm region of the spectrum. The purpose has been to better understand the different binding geometries that we have recently noticed between the DNA complexes with the  $\Delta$  and  $\Lambda$  enantiomers.<sup>10</sup> Our results indicate that the binding geometry, measured through the orientation and chromophoric perturbation of the complex, is almost the same for a given enantiomer irrespective of the kind of DNA. At the same time, variations in affinity between different combinations of enantiomers and DNAs suggest that the enantioselectivity is sensitively dependent on DNA sequence. This contrast in factors determining geometry and stereoselectivity is interesting in view of the current problems in understanding protein/DNA recognition.

## Materials and Methods

**Chemicals.**  $\text{RuCl}_3$  was purchased from Aldrich Chemical Co. Inc.  $[\text{Ru}(\text{phen})_3]^{2+}$  racemate was synthesized and resolved into optical isomers according to Dwyer and Gyrfas.<sup>14</sup> CD and absorption measurements were used to ensure chemical and enantiomeric purity. The samples

(1) Nordén, B.; Tjerneld, F. *FEBS Lett.* **1976**, *67*, 3, 368-370.

(2) Barton, J. K.; Dannenberg, J. J.; Raphael, A. L. *J. Am. Chem. Soc.* **1982**, *104*, 4967-4969.

(3) Barton, J. K. *J. Biomol. Struct. Dyn.* **1983**, *1*, 621-632.

(4) Barton, J. K.; Danishefsky, A. T.; Goldberg, J. M. *J. Am. Chem. Soc.* **1984**, *106*, 2172-2176.

(5) Kumar, C. V.; Barton, J. K.; Turro, N. J. *J. Am. Chem. Soc.* **1985**, *107*, 5518-5523.

(6) Barton, J. K.; Goldberg, J. M.; Kumar, C. V.; Turro, N. J. *J. Am. Chem. Soc.* **1986**, *108*, 2081-2088.

(7) Barton, J. K. *Science* **1986**, *233*, 727-734.

(8) Yamagashi, A. *J. Chem. Soc., Chem. Commun.* **1983**, 572-573.

(9) Hård, T.; Hiort, C.; Nordén, B. *J. Biomol. Struct. Dyn.* **1987**, *5*, 1, 1-8.

(10) Hiort, C.; Nordén, B. *Nucleosides Nucleotides* **1988**, *7*, 661-665.

(11) Hård, T.; Nordén, B. *Biopolymers* **1986**, *25*, 1209-1228.

(12) Goldstein, B. M.; Barton, J. K.; Berman, H. M. *Inorg. Chem.* **1986**, *25*, 842-847.

(13) Barton, J. K.; Basile, L. A.; Danishefsky, A.; Alexandrescu, A. *Proc. Natl. Acad. Sci. U.S.A.* **1984**, *81*, 1961-1965.

(14) Dwyer, F. P.; Gyrfas, E. C. *J. Proc. R. Soc. N.S.W.* **1949**, 170-173.

<sup>†</sup> Chalmers University of Technology.

<sup>‡</sup> Physical Chemistry Laboratory.

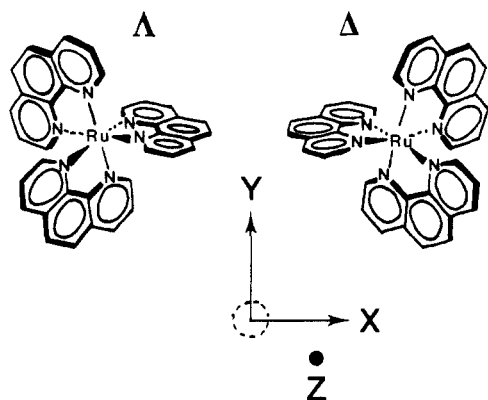


Figure 1. Absolute configurations of the  $\Delta$  and  $\Lambda$  enantiomers of  $[\text{Ru}(\text{phen})_3]^{2+}$  and the complex coordinate system ( $Z = C_3$  axis,  $X =$  one of the  $C_2$  axes). (Note that small letters are used in the text to denote the DNA coordinate system:  $z =$  helix axis;  $x =$  dyad axis.)

contained typically 95% of the enantiomer (+5% of the opposite enantiomer). The concentration of  $[\text{Ru}(\text{phen})_3]^{2+}$  in the pure metal complex solutions was determined from absorbance at 447 nm by using the molar absorptivity  $\epsilon_{447} = 19\,000 \text{ M}^{-1} \text{ cm}^{-1}$ .<sup>15</sup>

Calf thymus DNA (type 1) was purchased from Sigma. Double-stranded poly(dG-dC) and poly(dA-dT) were obtained from Pharmacia P-L Biochemicals, Uppsala, Sweden. DNA and  $[\text{poly}(\text{dA-dT})_2]$  were longer than 500 base pairs and gave sufficient flow orientation. With  $[\text{poly}(\text{dG-dC})_2]$ , though, the contour length was insufficient to give good orientation; however, by addition of dextran (1%), the viscosity was increased and the orientation considerably improved. All DNAs were used as they were obtained (identical spectroscopic and binding behavior with phenol-extracted DNA indicated that any remaining protein content was unimportant).<sup>11</sup> The concentrations of calf thymus DNA,  $[\text{poly}(\text{dA-dT})_2]$ , and  $[\text{poly}(\text{dG-dC})_2]$  were determined from light absorbance at 258 nm by using the molar absorptivities 6600, 8400, and 6600  $\text{M}^{-1} \text{ cm}^{-1}$ , respectively.<sup>16-18</sup> The samples were prepared in deionized and triply filtered distilled water (Millipore), either without buffer or in 0.01 M NaCl containing 0.001 M sodium cacodylate adjusted to pH 7. The metal complex stock solutions were kept in the dark to avoid photo-degradation.

**Linear Dichroism.** Linear dichroism (LD) is defined as the differential absorption of linearly polarized light

$$\text{LD}(\lambda) = A_{\parallel}(\lambda) - A_{\perp}(\lambda) \quad (1)$$

where  $\parallel$  and  $\perp$ , respectively, denote light polarized with its electric field vector parallel and perpendicular to the macroscopic orientation direction (flow direction). DNA was oriented between two concentric silica cylinders in a Couette flow cell,<sup>19,20</sup> and LD was measured on a Jasco J-500 spectropolarimeter modified and used as described elsewhere.<sup>21</sup> CD spectra were measured on the same instrument. The applied flow gradients were 1800  $\text{s}^{-1}$  for calf thymus DNA and 3000  $\text{s}^{-1}$  for the shorter polynucleotides. The "reduced LD" ( $\text{LD}^r$ ) was calculated as

$$\text{LD}^r(\lambda) = \text{LD}(\lambda) / A_{\text{iso}}(\lambda) \quad (2)$$

with  $A_{\text{iso}}$  representing the absorbance of the same isotropic sample (at rest). The isotropic absorbance was measured on a wavelength-matched Cary 219 spectrophotometer. The angles between the light-absorbing transition moments and the DNA helix axis are related to the corresponding  $\text{LD}^r$  according to<sup>22</sup>

$$\text{LD}^r = \frac{\sum f_i \epsilon_i(\lambda) \{\text{LD}^r\}_i}{\sum f_i \epsilon_i(\lambda)} \quad (3)$$

$$\{\text{LD}^r\}_i = \frac{3}{2} S (3 \langle \cos^2 \alpha_i \rangle - 1) \quad (4)$$

where  $\epsilon_i(\lambda)$  is the molar absorptivity of transition  $i$  at wavelength  $\lambda$ ,  $f_i$  is the fractional concentration of  $i$ , and  $S$  is an orientation factor.  $S = 1$  denotes perfect orientation with the helix axis parallel to the flow direction, and  $S = 0$  denotes random orientation.  $\alpha_i$  is the angle between the transition moment  $i$  and the helix axis, and  $\langle \cos^2 \alpha_i \rangle$  is an ensemble average.

**Orientation Factors.** For pure DNA,  $S$  is determined directly by measuring  $\text{LD}^r$  of the base absorption band at 258 nm by using an effective angle of 86°. <sup>23-26</sup> For a sample containing a very low concentration of metal complex, where in the UV region the LD and  $A_{\text{iso}}$  spectra contain negligible contributions from the metal complex absorption,  $S$  can be determined in the same way. When  $S$  is known for that sample, an LD per mole of bound metal complexes, at some wavelength where the spectrum is approximately (or exactly if there is an isosbestic point) invariant throughout the titration, can be obtained from the visible region of the spectrum by using

$$\text{LD}_m(\lambda) = \text{LD}(\lambda) / S C_B \quad (5)$$

where  $\text{LD}(\lambda)$  is the recorded LD and  $C_B$  is the concentration of bound molecules in the sample. The orientation factors for the rest of the samples are then calculated according to eq 5 by using appropriate  $\text{LD}(\lambda)$  and  $C_B$  values.

**Equilibrium Analysis.** The DNA/metal complex equilibria were studied with equilibrium dialysis. The dialysis was carried out over a membrane with a molecular weight cutoff of 6000 (Spectrapor). Equilibration was allowed to take place for at least 48 h at about 10 °C. The NaCl concentration was thereafter raised to 1 M, an ionic strength at which binding of the metal complexes to DNA is negligible.<sup>11</sup> The free and total metal complex concentrations  $[L]$  and  $C_L$ , respectively, were then determined spectrophotometrically in the solutions outside and inside the dialysis bag, respectively. The presence of DNA and salt was found not to affect the determination. The nucleotide concentration  $C_N$  was calculated from knowledge of the initial DNA concentration and of the volumes inside the dialysis bag before and after equilibration. The binding ratio  $r$  is defined as

$$r = (C_L - [L]) / C_N \quad (6)$$

The results are presented in terms of a Scatchard binding isotherm<sup>27</sup> or apparent stability constants defined as

$$K_{\text{app}} = \frac{C_B}{[L][\text{DNA site}]} = \frac{C_B}{[L](nC_N - C_B)} = \frac{r}{[L](n - r)} \quad (7)$$

where  $C_B$  is the concentration of the  $\text{Ru}(\text{phen})_3/\text{DNA}$  complex,  $[\text{DNA site}]$  the concentration of uncomplexed sites, and  $n$  the site density; by inference from the Scatchard plots,  $n$  is taken equal to 0.125 at low  $r$  values and 0.20 at high  $r$  values (equivalent to the respective stoichiometries 8 and 5 DNA bases per ligand).

**Preferentiality.** The preferentiality  $P$  is defined as the differential binding of the two enantiomers divided by the total amount of bound metal complex:

$$P = \frac{C_B(\Delta) - C_B(\Lambda)}{C_B(\Delta) + C_B(\Lambda)} \quad (8a)$$

The total amount of bound metal complex (denominator) was obtained from dialysis as  $C_L - [L]$ , whereas the difference in binding (numerator) was obtained from the CD ( $\text{CD}_{\text{out}}$ ) measured in the dialysate (outside the dialysis bag) by using

$$\begin{aligned} \text{CD}_{\text{out}} &= \text{CD}_{\text{out}}(\Delta) + \text{CD}_{\text{out}}(\Lambda) \\ &= \Delta\epsilon(\Delta)[\Delta] + \Delta\epsilon(\Lambda)[\Lambda] \\ &= \Delta\epsilon(\Delta)\{[\Delta] - [\Lambda]\} \end{aligned} \quad (8b)$$

and

(15) Lin, C.-T.; Böttcher, W.; Chou, M.; Creutz, C.; Sutin, N. *J. Am. Chem. Soc.* **1976**, *98*, 6536-6544.

(16) Felsenfeld, G.; Hirschman, S. Z. *J. Mol. Biol.* **1965**, *13*, 409-419.

(17) Wells, R. D.; Larson, J. E.; Grant, R. C.; Shortle, B. E.; Cantor, C. E. *J. Mol. Biol.* **1970**, *54*, 465-497.

(18) Inman, R. B.; Baldwin, R. L. *J. Mol. Biol.* **1962**, *5*, 172-184.

(19) Wada, A.; Kosawa, S. *J. Polym. Sci., Part A* **1964**, *2*, 853-864.

(20) Nordén, B.; Tjerneld, F. *Biophys. Chem.* **1976**, *4*, 191-198.

(21) (a) Davidsson, A.; Nordén, B. *Chem. Scr.* **1976**, *9*, 49-53. (b) Nordén, B.; Seth, S. *Appl. Spectrosc.* **1985**, *39*, 647-655. For a review on modulation spectroscopy with polarized light, see: (c) Schellman, J. A.; Jensen, H. P. *Chem. Rev.* **1987**, *87*, 1359-1399.

(22) Nordén, B. *Appl. Spectrosc. Rev.* **1978**, *14*, 157-248.

(23) Arnott, S.; Dover, S. D.; Wonacott, A. J. *Acta Crystallogr., Sect. B: Struct. Crystallogr. Cryst. Chem.* **1969**, *B25*, 2192-2206.

(24) Matsuoka, Y.; Nordén, B. *Biopolymers* **1982**, *21*, 2433-2452.

(25) Matsuoka, Y.; Nordén, B. *Biopolymers* **1983**, *22*, 1731-1746.

(26) Any static or dynamic extra inclination of the DNA bases is assumed to be on the average uniaxially symmetric and to be contained in the  $S$  factor. Curtis Johnson has found support for an unsymmetrical base inclination from vacuum ultraviolet LD measurements [Johnson, W. C. In *Polarized Spectroscopy of Ordered Systems*; Samori, B., Thulstrup, E. W., Eds.; NATO ASI, Kluwer Academic Publishers: Dordrecht, The Netherlands, 1988; pp 167-184], but this possibility will not be considered here, as it cannot significantly influence the conclusions.

(27) Scatchard, G. *Ann. N.Y. Acad. Sci.* **1949**, *51*, 660-670.

$$V_{\text{in}}C_{\text{B}}(\Delta) + V_{\text{in}}[\Delta] + V_{\text{out}}[\Delta] = V_{\text{in}}C_{\text{B}}(\Lambda) + V_{\text{in}}[\Lambda] + V_{\text{out}}[\Lambda]$$

which gives

$$\text{CD}_{\text{out}} = -\Delta\epsilon(\Delta)(V_{\text{in}}/V_{\text{tot}})(C_{\text{B}}(\Delta) - C_{\text{B}}(\Lambda)) \quad (8c)$$

where  $[\Delta]$ ,  $[\Lambda]$ ,  $C_{\text{B}}(\Delta)$ , and  $C_{\text{B}}(\Lambda)$  denote free and bound concentrations of the respective enantiomers and  $\Delta\epsilon$  is the differential molar absorptivity of circularly polarized light ( $\Delta\epsilon = \epsilon_{\text{L}} - \epsilon_{\text{R}}$ ).  $V_{\text{in}}$  and  $V_{\text{out}}$  are the sample volumes inside and outside the dialysis bag.

**Theory.** Polarized light spectroscopy can be an effective tool for probing an interaction between an adduct molecule and DNA if the interaction is a small perturbation and the combined system can be described, from perturbation theory, in terms of the properties (e.g., transition moments) of the isolated molecules. Expressions for the changes in  $A_{\text{iso}}$  and CD and for the linear dichroism (LD) for electric-dipole-allowed (eda) transitions are derived in the Appendix by this approach. In the  $D_3$  complexes studied in this work, eda transitions with  $A_2$  or E symmetry can occur, i.e., with transition moments Z- and XY-polarized, respectively. In  $[\text{Ru}(\text{phen})_3]^{2+}$  the intense eda charge-transfer absorption envelope at 350–550 nm thus includes both E and  $A_2$  transitions, with the  $A_2$  transition located at the longer wavelength. The charged backbone of the DNA is found to have no important effect on the  $A_2$  eda transitions of the metal complex (its effect on the E transition is only briefly considered). Let us consider the interaction of one complex with DNA. As discussed in the Appendix, we may limit our representation of DNA to in-plane polarized base-pair transitions.<sup>24,25,28</sup> The Z axis of the metal complex is defined to be the 3-fold axis (Figure 1). We choose X to be one of the 2-fold rotation axes. The system origin is taken to be the metal atom. The LD experiment defines the z axis of the complex/DNA system to be the unique direction of orientation, i.e., the DNA helix axis. The x axis is taken to be the line perpendicular to z that passes through the metal. The right-handed axis system for the metal complex,  $\{X, Y, Z\}$ , and the right-handed axis system for DNA,  $\{x, y, z\}$ , are related by a unitary transformation such that  $X = (\alpha, \beta, \gamma)$ ,  $Y = (\delta, \epsilon, \zeta)$ , and  $Z = (\eta, \theta, \kappa)$ . We take the direction cosines  $\alpha \geq 0$  and  $\kappa \geq 0$ , thus specifying the directions of the axes of the complex (unless  $\alpha = 0$ , or  $\kappa = 0$ , in which case take  $\beta \geq 0$  or  $\theta \geq 0$ ). We define the unit vector from the metal atom toward a base-pair origin to be  $\rho = (-s, 0, t)$ ;  $s \geq 0$ . Since no base-pair transitions parallel to z need be considered (see Appendix), the following expressions for the  $A_{\text{iso}}$  and CD changes [ $\delta(I)$  and  $\delta(R)$ , respectively] and the LD of eda transitions of a metal complex in the presence of DNA result from eqs A7–A9 of the Appendix:

$$\delta(I, A_2) = -\frac{4\epsilon_b}{3(\epsilon_b^2 - \epsilon_1^2)r^2} [\mu(A_2)_2](\eta B_x + \theta B_y) [(1 - 3s^2)\eta B_x + \theta B_y + 3st\kappa B_x] \quad (9)$$

$$\delta(I, X) = -\frac{4\epsilon_b}{3(\epsilon_b^2 - \epsilon_1^2)r^2} [\mu(X)^2](\alpha B_x + \beta B_y) [(1 - 3s^2)\alpha B_x + \beta B_y + 3st\gamma B_x] \quad (10)$$

$$\delta(I, Y) = -\frac{4\epsilon_b}{3(\epsilon_b^2 - \epsilon_1^2)r^2} [\mu(Y)^2](\delta B_x + \epsilon B_y) [(1 - 3s^2)\delta B_x + \epsilon B_y + 3st\zeta B_x] \quad (11)$$

$$\text{LD}(A_2) = \frac{1}{2}[\mu(A_2)^2(3\kappa^2 - 1) - \delta(I, A_2)]S \quad (12)$$

$$\text{LD}(X) = \frac{1}{2}[\mu(X)^2(3\gamma^2 - 1) - \delta(I, X)]S \quad (13)$$

$$\text{LD}(Y) = \frac{1}{2}[\mu(Y)^2(3\zeta^2 - 1) - \delta(I, Y)]S \quad (14)$$

$$\text{LD}(E) = \frac{1}{2}[\frac{1}{2}[\mu(X)^2 + \mu(Y)^2](1 - 3\kappa^2) - \delta(I, E)]S \quad (15)$$

$$\delta(R, A_2) = -\frac{\epsilon_1\epsilon_b 4\pi}{h(\epsilon_b^2 - \epsilon_1^2)r^2} \mu(A_2)^2 [(1 - 3s^2)\eta B_x + \theta B_y + 3st\kappa B_x] (-\eta t B_y + \theta t B_x - \kappa s B_y) \quad (16)$$

$$\delta(R, X) = -\frac{\epsilon_1\epsilon_b 4\pi}{h(\epsilon_b^2 - \epsilon_1^2)r^2} \mu(X)^2 [(1 - 3s^2)\alpha B_x + \beta B_y + 3st\gamma B_x] (-\alpha t B_y + \beta t B_x - \gamma s B_y) \quad (17)$$

$$\delta(R, Y) = -\frac{\epsilon_1\epsilon_b 4\pi}{h(\epsilon_b^2 - \epsilon_1^2)r^2} \mu(Y)^2 [(1 - 3s^2)\delta B_x + \epsilon B_y + 3st\zeta B_x] (-\delta t B_y + \epsilon t B_x - \zeta s B_y) \quad (18)$$

where  $\mu(A_2)^2$  denotes the dipole strength of a Z( $A_2$ )-polarized unper-

turbed complex transition,  $B_x$  is the x component of the DNA-base transition moment  $\mu_b^{0b}$  (similarly  $B_y$  and  $B_z$ ),  $\epsilon_b$  is the transition energy of  $\mu_b^{0b}$ ,  $\epsilon_1$  is the energy of the complex transition of interest, and summation over base pairs and base-pair transitions is implied. We shall later compare the theoretical predictions for an E transition with the experimental spectra to see whether or not it is appropriate to consider the X/Y degeneracy of the complex to be retained upon binding to DNA.

Rearranging eq 12 and substituting measurable quantities, such as  $3C_{\text{B}}\epsilon_{\text{F}}$  for  $\mu(A_2)^2$  and  $I(A_2)_{\text{meas}} - \epsilon_{\text{F}}[L] + C_{\text{B}}$  for  $\delta(I, A_2)$ , result in a convenient form for the direction cosine,  $\kappa$ :

$$\kappa = \left[ \frac{2[\text{LD}(A_2)_{\text{meas}}/S] - 3[L]\epsilon_{\text{F}} + 3I(A_2)_{\text{meas}}}{9C_{\text{B}}\epsilon_{\text{F}}} \right]^{1/2} \quad (19)$$

where  $\text{LD}(A_2)_{\text{meas}}$  and  $I(A_2)_{\text{meas}}$  are respectively the total LD and total  $A_{\text{iso}}$  of the  $A_2$  band at the same wavelength and the same concentration of the metal complex (bound + free),  $[L]$  is the concentration of the free complex in solution,  $C_{\text{B}}$  is the concentration of the bound complex, and  $\epsilon_{\text{F}}$  is the molar absorptivity of the free complex at the same wavelength as the intensity measurements.  $\mu(A_2)^2 = 3I(A_2)$  (due to rotational averaging and assuming no E intensity at the wavelength chosen), and S is the orientation factor discussed earlier. It should be recalled that  $\kappa^2$  in fact represents an average ( $\langle \kappa^2 \rangle$ ) over the particular angular distribution just as in eq 4. Note that our perturbation treatment implies that a chromophore oriented at the magic angle so that  $3\kappa^2 - 1$  is zero does not necessarily show zero linear dichroism, as would have been expected from the classical expressions for dichroism.<sup>20–22</sup> The extra contribution (below called hyperchromic dichroism) can be regarded as arising from perturbation of the observed transition owing to interaction with transitions of surrounding DNA chromophores. As seen from eq 19, this contribution for the  $A_2$  band is in our approach directly related to the change in normal absorption upon binding to DNA, i.e., to  $\delta(I)$ . It may clearly be a substantial effect that has to be corrected for in the calculation of  $\kappa$ , and as will be inferred below, this is a main source of the difference in features between the LD spectra of the two enantiomers when bound to DNA.

## Results

Figure 2 shows representative isotropic absorption ( $A_{\text{iso}}$ ), linear dichroism (LD), and circular dichroism (CD) spectra for calf thymus DNA solutions containing  $\Delta$  and  $\Lambda$  enantiomers (and also the racemate) of  $[\text{Ru}(\text{phen})_3]^{2+}$  in the region of the complex CT band, the low-lying base-pair transitions, and the first intraligand transitions. In Figures 3 and 4 correspondingly, the spectra are shown for the mixtures with the polynucleotides  $[\text{poly}(\text{dA-dT})]_2$ , denoted below as AT, and  $[\text{poly}(\text{dG-dC})]_2$ , denoted GC. Owing to the short contour length of most of the preparation batches of  $[\text{poly}(\text{dG-dC})]_2$ , this polynucleotide was difficult to orient in aqueous solution, and upon interaction with the metal complexes, the orientation was further impaired so that the LD vanished. However, by adding dextran (approximately 1%) to increase the viscosity of the solution, we obtained measurable flow LD both in the nucleotide and in the metal complex absorption regions. To check that dextran did not alter the DNA conformation or binding geometry, the  $[\text{poly}(\text{dA-dT})]_2$  samples were run both in aqueous and in dextran solutions (Figure 3) and were found to give essentially the same spectral features (a base-line problem, though, makes the dextran experiments difficult to interpret quantitatively).

**$A_{\text{iso}}$ .** In a solution of DNA and metal complex, the magnitude and shape of the visible absorption band are noticeably changed compared with the pure metal complex spectrum. For both  $\Delta$  and  $\Lambda$ , the intensity around 450 nm decreases by approximately 15% and the structured profile is smoothed upon binding to DNA. At the low-energy side of the absorption spectrum, the intensity increases by some 15%. The spectral changes are slightly different for the two enantiomers.

**LD.** The LD spectra are due *totally* to the interaction of the complexes with DNA. Upon interaction with flow-oriented calf thymus DNA, the  $\Delta$  enantiomer displays two LD bands of comparable magnitudes and opposite signs in the visible charge-transfer (CT) region of the spectrum (Figure 2), at 470 and 380 nm. In addition, there is a shoulder on the high-energy side of the negative peak, at about 430 nm. The  $\Lambda$  enantiomer shows one strong, structured positive band at 425 nm and a very small negative indication at 480 nm. The substantial differences observed for

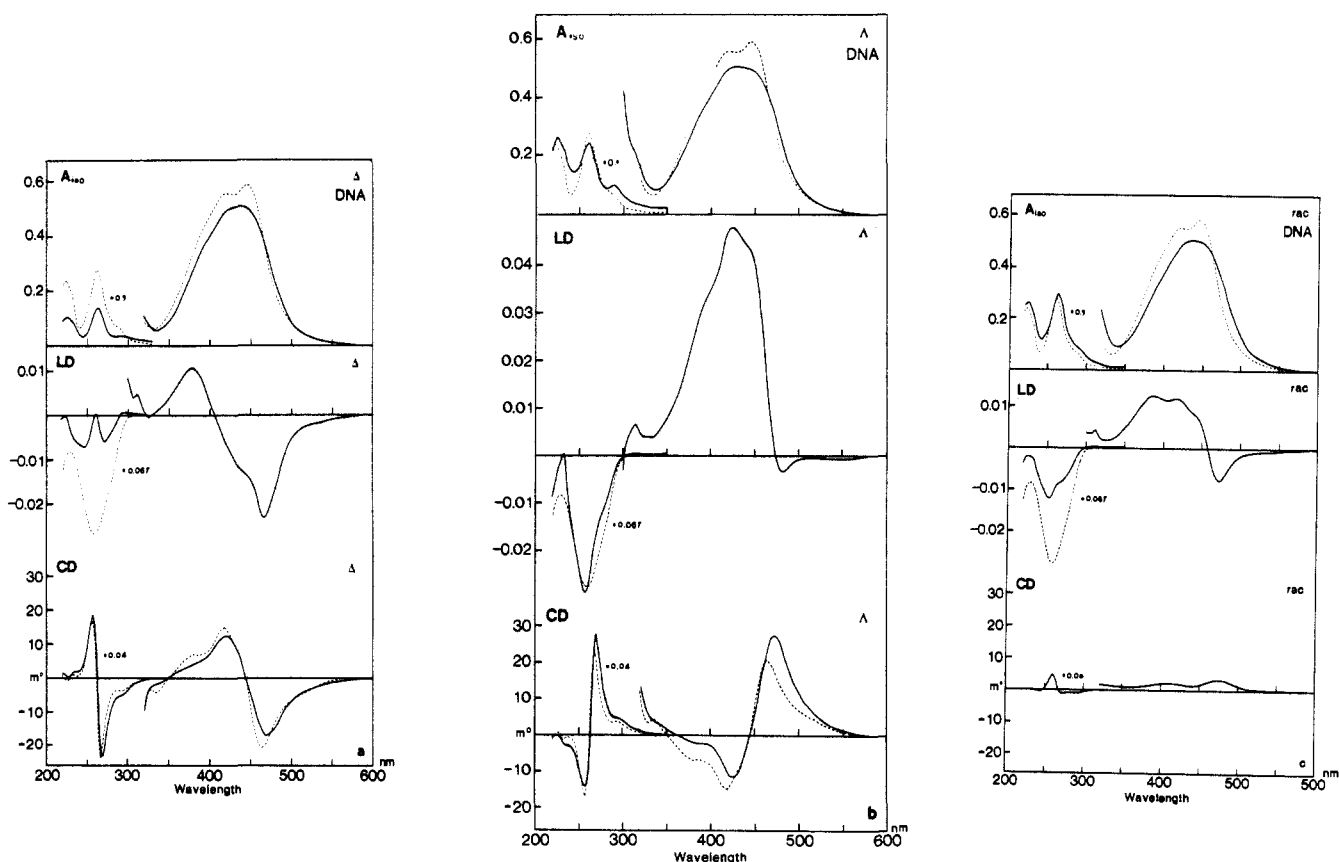


**Figure 2.** Normal absorption ( $A_{180}$ ), linear dichroism (LD), and circular dichroism (CD) spectra of (a)  $\Delta$ , (b)  $\Lambda$ , and (c) racemic  $[\text{Ru}(\text{phen})_3]^{2+}$  in the presence of DNA. In the  $A_{180}$  and CD spectra, contributions from DNA and the free metal complex have been subtracted (broken curves show  $A_{180}$  and CD of the free metal complex and the LD of pure DNA). The total concentrations of the metal complex and DNA phosphate were in all samples 31 and 400  $\mu\text{mol L}^{-1}$ , respectively. All spectral intensities are in absorbance units and normalized to 1-cm optical path length.

the LD spectra of the  $\Delta$  and  $\Lambda$  complexes indicate different binding geometries and/or different extents of perturbation of the complexes upon association with DNA.

Figures 3 and 4 show corresponding spectra for the AT and GC polynucleotides. The LD spectra obtained for each enantiomer in the presence of AT, GC, and DNA are almost the same, demonstrating that  $\Delta$ - and  $\Lambda$ - $[\text{Ru}(\text{phen})_3]^{2+}$  bind to all three DNAs with essentially the same binding geometry. The LD spectra with GC differed somewhat from the other spectra, which can be attributed to the dextran that had to be added to obtain measurable signals (cf. the effect of dextran in Figure 3a).

Figure 5 shows the LD spectrum of racemic  $[\text{Ru}(\text{phen})_3]^{2+}$  in the presence of DNA. When the LD spectrum of the  $\Delta$  enantiomer bound to DNA is subtracted from the racemic spectrum, a virtually pure  $\Lambda$ /DNA spectrum can be obtained. This observation of perfect superposition of spectra shows that the two enantiomers do not affect each other's spectral properties even when bound to DNA at the same time.

**CD.** The changes in the visible region of the CD spectrum of  $\Lambda$ - $[\text{Ru}(\text{phen})_3]^{2+}$  upon binding to all three types of DNA consist of positive contributions to both the positive long-wavelength (>470 nm) and the negative short-wavelength (420 nm) CD bands. For the  $\Delta$  enantiomer, the CD maxima at 470 and 425 nm show a positive change in the long-wavelength region and a negative change in the short-wavelength region, respectively. With a racemic mixture, which has no CD in the absence of DNA, an overall positive CD in the CT region is observed in the presence of all three DNAs. The amplitude of the racemic CD varies with the type of DNA. In the UV region of the CD spectra of both enantiomers, changes corresponding to those in the CT region are seen.

**LD Titrations—Isosbestic Points.** In order to search for variations in binding geometry with varying degrees of occupancy, we have studied the shape of the LD spectra at different metal complex/DNA mixing ratios and also at different ionic strengths.

The results are shown for both DNA and  $[\text{poly}(\text{dA-dT})_2]_2$  in Figure 6 (complex titrations) and Figure 7 (salt titrations). In Figure 6a–c (calf thymus DNA), the particular binding ratios have been determined from dialysis experiments. For both  $\Delta$  and  $\Lambda$  in the presence of the AT polynucleotide, clear isosbestic points and constant *spectral* proportions (ratio between long- and short-wavelength bands, at 415 and 472 nm, respectively) indicate a single oriented binding mode for each of the complexes over a large range of binding ratios. With DNA, however, the absence of isosbestic behavior for  $\Lambda$ , and an only approximate isosbestic point with  $\Delta$  (at about 405 nm; see Figure 6a), shows that the binding is at least geometrically heterogeneous. With the racemate, not unexpectedly, no isosbestic point is ever observed.

The behavior in Figure 7, where increasing amounts of salt are added to DNA/metal complex solutions of fixed composition, is practically the same as that in Figure 6, showing that the only effect of ionic strength is to change the effective binding ratio. This is in accordance with our conclusion (Appendix) of a negligible optical perturbation from the charged DNA backbone.

In Figure 8, the behavior of the isotropic absorption spectrum of the enantiomers (constant total concentration) at various DNA concentrations is illustrated. Isosbestic points (arrows) are observed at 466 nm (and also at 353 nm) for  $\Delta$  and at 463 nm (and 344 nm) for  $\Lambda$ , in the normal absorption, in contrast to the apparently more sensitive LD results. With AT, corresponding isosbestic points are observed (results not shown) at 471 and 341 nm for  $\Delta$  and 465 and 335 nm for  $\Lambda$ . With the racemate, no isosbestic points are observed for DNA and AT. Interestingly, no pure isosbestic points are observed for either of the enantiomers with GC (results not shown).

**Effect of Complexation on DNA Orientation.** In Figure 6a, a marked decrease of the LD in the region of the DNA base absorption suggests that the  $\Delta$  complex reduces the DNA orientation (orientation factor  $S$ ). In contrast, the  $\Lambda$  complex only slightly affects the DNA orientation. These deductions are confirmed

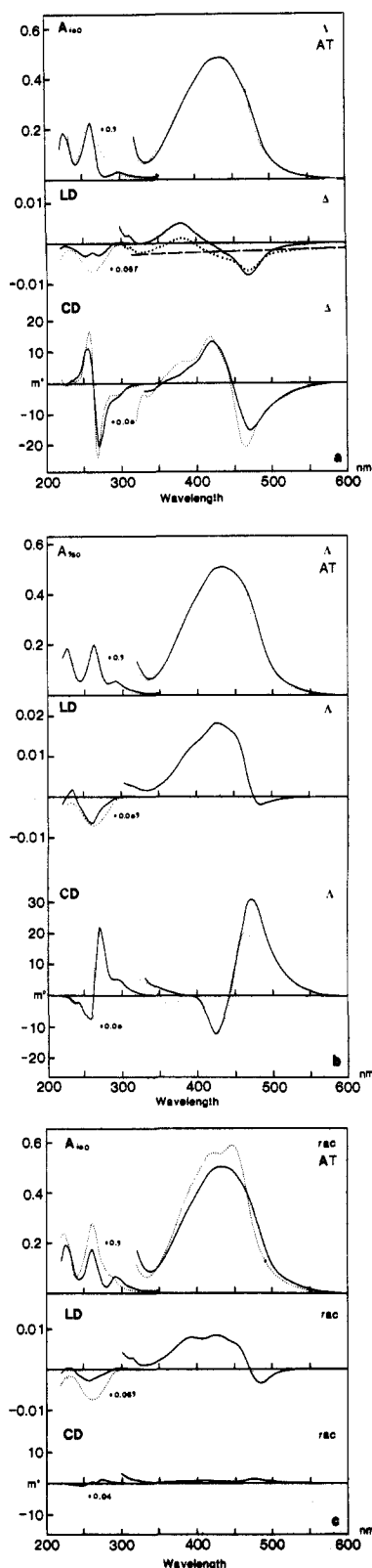


Figure 3.  $A_{180}$ , LD, and CD spectra of (a)  $\Delta$ , (b)  $\Lambda$ , and (c) racemic  $[\text{Ru}(\text{phen})_3]^{2+}$  in the presence of  $[\text{poly}(\text{dA-dT})]_2$ . All concentrations and other conditions were as in Figure 2. In LD, in the region 300–600 nm of panel a, a dotted curve shows an LD spectrum recorded in the presence of 1% dextran.

by Figure 9, which shows  $S$  obtained from the metal complex LD on the assumption of a constant binding geometry. This assumption is justified for the  $\Delta$  complex by its isosbestic behavior, and for the  $\Lambda$  isomer an approximate value of  $S$  was obtained in the 400-nm region, where the shape of the LD spectrum appears invariant.

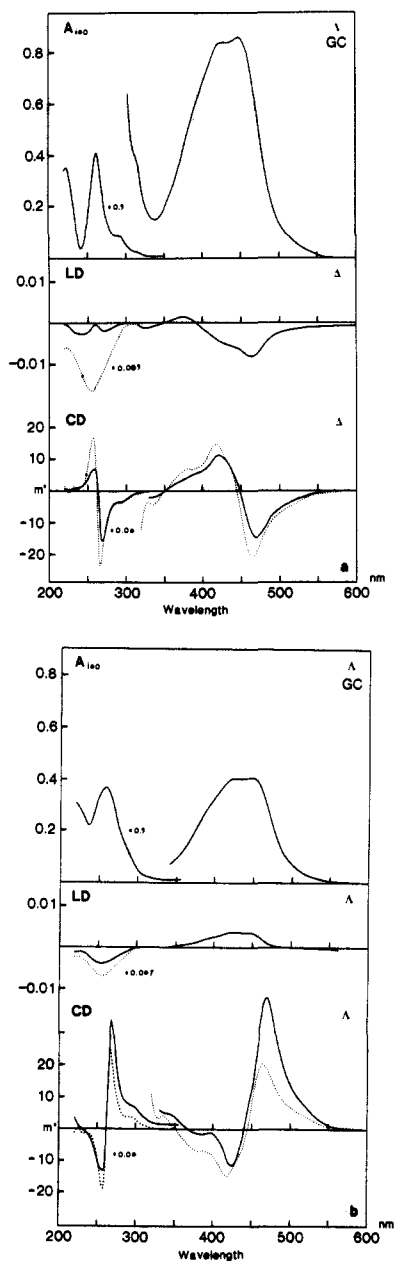


Figure 4.  $A_{180}$ , LD, and CD spectra of (a)  $\Delta$ - and (b)  $\Lambda$ - $[\text{Ru}(\text{phen})_3]^{2+}$  in the presence of  $[\text{poly}(\text{dG-dC})]_2$ . The LD spectra (and also  $A_{180}$ ) were recorded in 1% dextran (the metal complex concentrations were  $50 \mu\text{M}$  for  $\Delta$  and  $20 \mu\text{M}$  for  $\Lambda$ ). Other conditions were as in Figure 2.

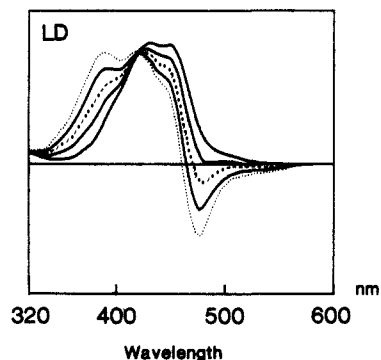
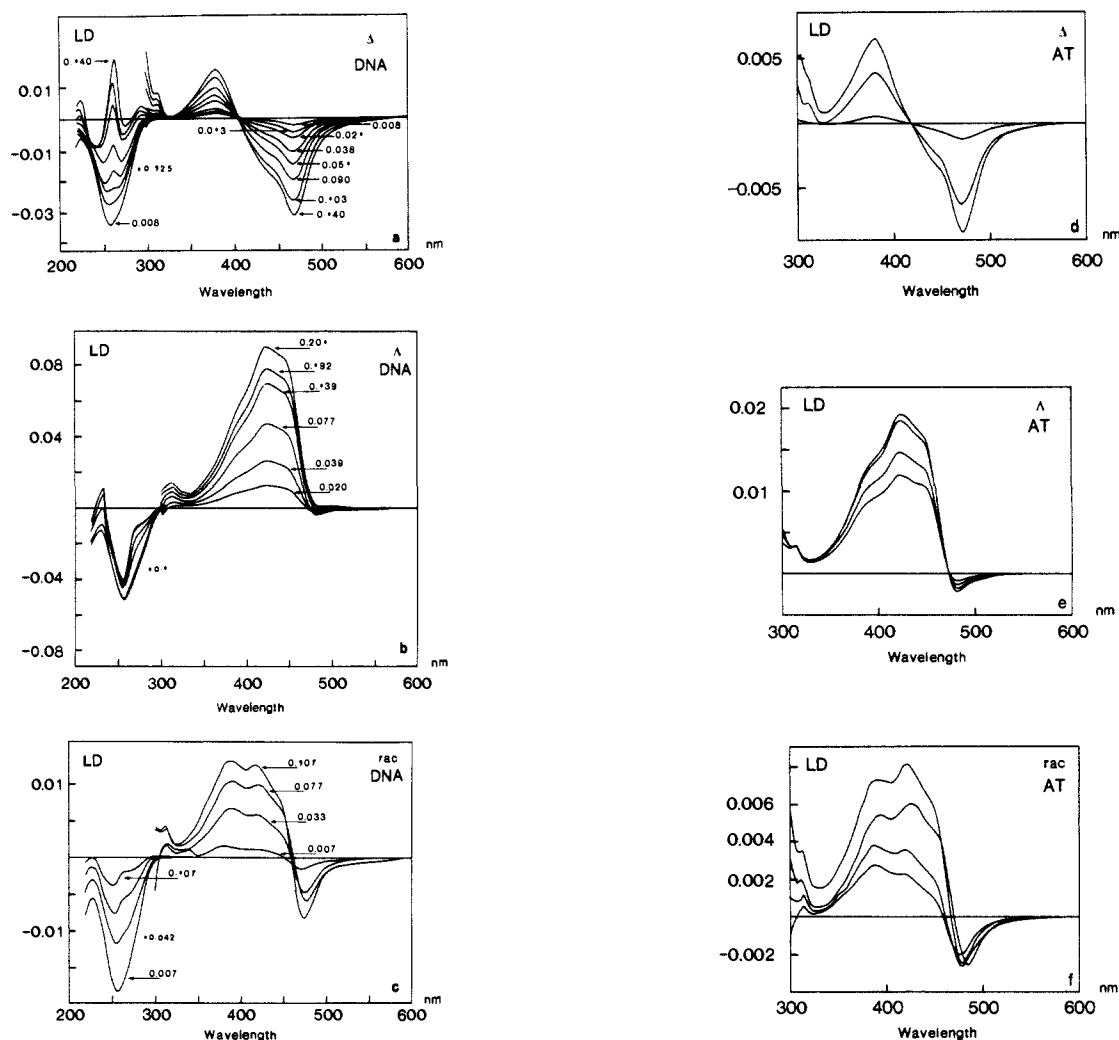


Figure 5. Some linear combinations of the observed LD spectra of  $\Delta$  + DNA and racemate + DNA: the broken curve has a shape that may be identified with the  $\Delta$  + DNA spectrum; see Figure 2.

An independent check of the DNA orientation was obtained by measuring the LD on a probe (the dye methylene blue) that is known to intercalate parallel to the base planes.<sup>29</sup> Only a very



**Figure 6.** LD spectra of  $[\text{Ru}(\text{phen})_3]^{2+} + \text{DNA}$  at different adduct/nucleotide binding ratios,  $r$ : (a)  $\Delta$ , (b)  $\Lambda$ , and (c) racemate. Binding ratios, determined by equilibrium dialysis, are given in the figure for DNA ( $C_N = 0.36 \text{ mM}$ ). Corresponding LD spectra with  $[\text{poly}(\text{dA-dT})]_2$  are shown in panels d, e, and f.

**Table I.** Apparent Stability Constants<sup>a</sup> at Low and High Binding Ratios Determined from Equilibrium Dialysis

bases	$K_{\text{app}}/10^{-6} \text{ M}^{-1}$ ( $r$ in parentheses) for the complex			$C_L/\mu\text{M}$
	$\Delta$	racemate	$\Lambda$	
AT	$1.03 \pm 0.05$ (0.046)	$1.95 \pm 0.05$ (0.061)	$2.45 \pm 0.60$ (0.068)	5
	$0.16 \pm 0.03$ (0.115)	$0.18 \pm 0.03$ (0.124)	$0.48 \pm 0.10$ (0.147)	25
DNA	$1.54 \pm 0.13$ (0.048)	$0.95 \pm 0.23$ (0.041)	$1.17 \pm 0.05$ (0.040)	5
	$0.27 \pm 0.04$ (0.125)	$0.14 \pm 0.03$ (0.111)	$0.63 \pm 0.08$ (0.143)	25
GC	$1.27 \pm 0.05$ (0.065)	$1.25 \pm 0.05$ (0.056)	$0.88 \pm 0.13$ (0.037)	5
	$0.61 \pm 0.16$ (0.160)	$0.30 \pm 0.05$ (0.144)	$0.35 \pm 0.05$ (0.146)	25

<sup>a</sup> Calculated according to eq 7;  $C_N = 0.36 \text{ mM}$ .

small amount of probe was added so as not to disturb the structure and complexation of DNA. The result (shown as separate points in Figure 9) verifies the  $S$  values obtained from the metal complex LD.

**Binding Affinities.** A Scatchard plot based on dialysis experiments with the  $\Delta$  and  $\Lambda$  complexes in the presence of DNA (Figure 10a) did not reveal with any accuracy which of the enantiomers has the stronger DNA affinity. The average binding constant and site density ( $K = 40\,000 \text{ M}^{-1}$ ,  $n = 0.10\text{--}0.15$  in  $0.01 \text{ M NaCl}$ ) are, given the lower ionic strength in our experiments, consistent with dialysis results on the racemate reported by Barton<sup>4</sup> ( $K = 6200 \text{ M}^{-1}$ ,  $n = 0.125$  at  $0.05 \text{ M NaCl}$ ).

In Figure 10b, the enantiomeric excess upon interaction of the racemate with AT, DNA, and GC is shown. The results were

obtained from CD measurements on the dialysate resulting from dialysis at a constant complex concentration. The complex concentration was selected to give binding ratios below saturation, yet still accurately determinable.

The problem with poor accuracy of the stability constants determined from the Scatchard plot was circumvented by calculating "apparent stability constants" by adopting a fixed density of binding sites, according to eq 7, which allows comparison of the relative binding affinities of the various combinations of enantiomers and DNAs. The results from the dialysis experiments, summarized in Table I, show that in the region of low binding ratios ( $\approx 0.05$ ) the order of binding affinities is

$$\Lambda/\text{GC} < \Delta/\text{AT} < \Lambda/\text{DNA} < \Delta/\text{GC} < \Delta/\text{DNA} < \Lambda/\text{AT}$$

whereas at higher binding ratios  $\Delta/\text{DNA}$  becomes weaker and  $\Lambda/\text{DNA}$  stronger.

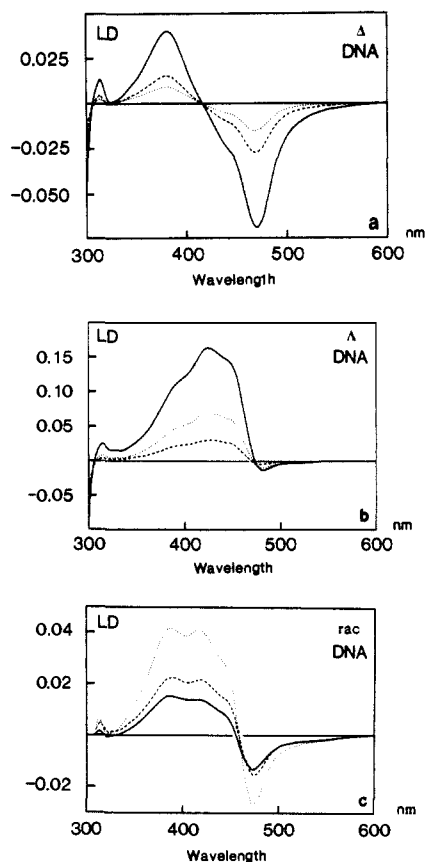


**Figure 7.** LD spectra of DNA +  $[\text{Ru}(\text{phen})_3]^{2+}$  solutions ( $C_L = 50 \mu\text{mol L}^{-1}$ ), (a)  $\Delta$ , (b)  $\Lambda$ , and (c) racemate, at different ionic strengths. In (a), 0 (—), 30 (---), and 150 (---) mM NaCl; in (b), 0 (—), 30 (---), and 150 (---) mM NaCl; in (c), 0 (---), 30 (---), and 150 (—) mM NaCl.

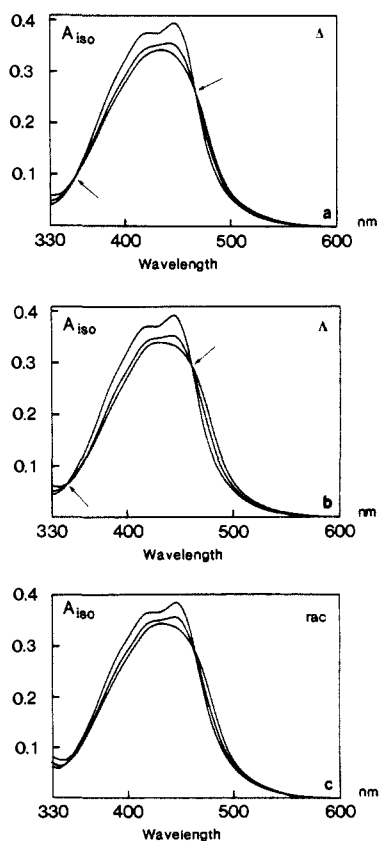


**Figure 8.** Representative  $A_{\text{iso}}$  spectra of DNA +  $[\text{Ru}(\text{phen})_3]^{2+}$ : (a)  $\Delta$ , (b)  $\Lambda$ , and (c) racemate.  $C_L$  was kept constant, equal to  $20 \mu\text{M}$ . Arrows show isosbestic points (for clarity reasons only a few selected spectra are shown).

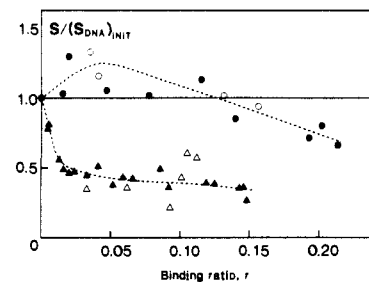


**Figure 9.** DNA orientation at different adduct/nucleotide binding ratios ( $r$  determined by equilibrium dialysis). The orientation factor  $S$  is normalized with respect to the initial value (DNA in the absence of adduct). Circles and triangles denote  $\Lambda + \text{DNA}$  and  $\Delta + \text{DNA}$  samples, respectively. Open symbols denote the  $S$  values obtained by using intercalated methylene blue as a probe of base-pair orientation.

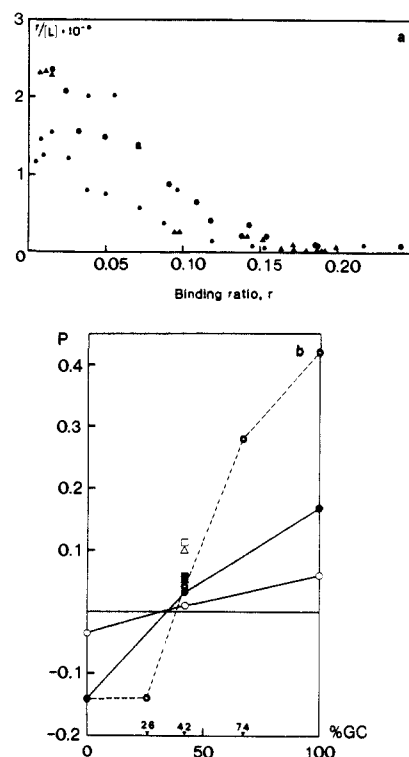


**Figure 10.** (a) Scatchard plot of  $[\text{Ru}(\text{phen})_3]^{2+}$  binding to DNA ( $C_N = 0.36 \text{ mM}$ ). The binding ratio,  $r$ , and free adduct concentration,  $[L]$ , were determined by equilibrium dialysis. Circles and triangles denote  $\Lambda + \text{DNA}$  and  $\Delta + \text{DNA}$  systems, respectively. (b) Preferentiality in binding of  $\Delta$ - $[\text{Ru}(\text{phen})_3]^{2+}$  to DNA of varying GC content determined through equilibrium dialysis at high ( $25 \mu\text{M}$ , filled symbols) and low ( $5 \mu\text{M}$ , open symbols) total ruthenium concentrations. Circles, squares, and triangles denote 0, 10, and 30 mM NaCl, respectively. Also shown for comparison are the results reported by Barton et al.<sup>6</sup> in 50 mM NaCl (points on broken curve).

## Discussion

A central message of this study is the information about binding geometry provided by the flow linear dichroism spectra of the metal complexes when associated with DNA. As will be inferred, the  $\Delta$  and  $\Lambda$  forms of  $[\text{Ru}(\text{phen})_3]^{2+}$  exhibit individual binding modes that are characterized by an average inclination of the  $C_3$  axis relative to the DNA helix axis of approximately  $70^\circ$  and  $50^\circ$ , respectively. Furthermore, the LD spectra have characteristic profiles owing to dispersive perturbation from the DNA chromophores. Surprisingly enough, these spectral features are virtually independent of the kind of DNA with which the respective enantiomer is associated. This suggests that the mode of binding, including the geometry, is determined by the nonspecific "texture", i.e., the helical sense and pitch of DNA, irrespective of base sequence. In contrast, the two enantiomers show binding affinities and stereopreferentialities that vary considerably with base com-

position and even with the degree of association and ionic conditions.

**Linear Dichroism.** There are two possible contributions to the metal complex LD: (i)  $LD^0$  = the *orientational* LD, due purely to the nonrandom orientation of  $\Delta$  and  $\Lambda$  by DNA, and (ii)  $LD'$  = the *hyperchromic* LD, due to the perturbation of the enantiomers by DNA. If (ii) were not present, the  $\Delta$  and  $\Lambda$  enantiomers, even if on different binding sites, should have  $LD(\Delta)/LD(\Lambda) = g$ , where  $g$  is a geometrical factor; i.e., their LD spectra should have the same shape, which is clearly not the case (cf. Figure 2). If (i) were not present, the LD would be due to a purely dispersive rotationally averaged interaction and the LD spectra for  $\Delta$  and  $\Lambda$  would be identical.<sup>30</sup> Thus, the different LD spectra observed in the metal complex absorption bands for the  $\Delta$  and  $\Lambda$  enantiomers upon association with flow-oriented DNA mean that both enantiomers bind to DNA in preferential nonrandom geometries and that at least one of them exhibits hyperchromic LD.

As each of the enantiomers has practically identical LD spectra when bound to DNA, AT, or GC, despite markedly varying binding affinities, we can conclude that the binding geometries in different DNAs are essentially the same but differ between  $\Delta$  and  $\Lambda$ . The approximate isosbestic point obtained when the amount of  $\Delta$  bound to DNA is increased over a large range of binding ratios ( $\leq 0.15$ ) indicates a single binding geometry of  $\Delta$  on DNA. This is confirmed in the ionic strength study, which shows a perfect isosbestic behavior; cf. Figure 7. By contrast, the absence of an isosbestic point with  $\Lambda$ /DNA indicates binding heterogeneity. This could be due to different binding sites or different binding geometries or to intercomplex interactions at higher degrees of binding. The observation of a distinct isosbestic point in  $\Lambda$ /AT indicates that the effect is not due to *intercomplex* interaction. As the small negative  $A_2$  band at 480 nm (see below for assignment) does not need very much perturbation to appear nonisosbestic and the normal absorption is not sensitive enough to detect the heterogeneity, it is likely that this heterogeneity in binding is small.

In contrast to these conclusions, Barton has, on the basis of fluorescence and unwinding results, proposed that both of the  $[Ru(phen)_3]^{2+}$  enantiomers display two DNA binding modes: one involving intercalation and one surface binding.<sup>2,4-6</sup> In light of the distinct isosbestic points that we have observed in the LD spectra for the  $\Delta$  enantiomer in general and for  $\Lambda$  with AT, over a wide range of binding ratios, if a surface binding mode is operative, it must be completely orientationally unspecific. However, the observation of largely the same ratio  $LD/rS$  at low and high  $r$  values does not indicate any increasing amounts of unoriented metal complex with higher  $r$  values, as would be expected if surface binding were taking over. Still, our isosbestic LD behavior does not definitely exclude the coexistence of two binding modes, since the ratio of the bound forms (intercalated and surface bound) might remain constant with the degree of binding. However, an isosbestic behavior is also observed with ionic strength (Figure 7). If this were due to a constant ratio of the bound forms, it would require the same free energy changes for both binding modes upon changing ionic strength. This seems improbable, since one may anticipate that the electrostatic contributions to the binding energies should differ significantly between intercalated and surface modes.

The studies on the racemate indicate that at least some  $\Delta/\Lambda$  competition for binding sites on AT, since the racemic (50%  $\Delta$  + 50%  $\Lambda$ ) metal complex plus AT gives an LD spectrum that is a combination of the pure  $\Delta$  and  $\Lambda$  spectra at low binding ratios and at higher binding ratios (where the  $\Lambda$ /AT greater binding affinity becomes significant) becomes more  $\Lambda$ -like (Figure 6e). When racemate is added to DNA, the LD spectrum remains "racemic", with a slight excess of  $\Delta$ , over the whole range of binding ratios (Figure 6a). This is consistent with the stronger binding affinity of  $\Delta$  for DNA at low binding ratios (Table I), but with a higher stability constant for  $\Lambda$  at higher binding ratios

one would expect a more  $\Lambda$ -like spectrum, as is the case for AT.

The DNA LD band ( $LD_{260nm}$ ) decreases markedly when  $\Delta$  is added, indicating a decrease in DNA orientation. The drop-off in  $S$  for  $\Delta$ /DNA is particularly sharp at low metal/DNA binding ratios, which is consistent with a perturbation of the DNA structure that is either a static (a kink) or a flexibility increase caused, for example, by electrostatic screening or steric interactions. By contrast, the  $\Lambda$  complex, which one might expect to have the same effect, only slightly perturbs the DNA LD, in fact initially increasing it.

**Circular Dichroism.** The CD in the CT bands of the metal complexes changes upon binding, owing to a structural or spectroscopic perturbation by the DNA. The changes ( $\delta CD$ ) are numerically similar but of different signs for  $\Delta$  and  $\Lambda$ . The CD of the racemate can be explained as  $\delta CD_{\Delta} + \delta CD_{\Lambda}$ . This additivity gives no indication of spectroscopic interaction between bound enantiomers, in support of the LD results. That the residual CD does not cancel to zero for the racemate in the presence of DNA is due to one of the following: different amounts of  $\Delta$  and  $\Lambda$  are bound to DNA and there is no difference in perturbation of the enantiomers by DNA, or the same amounts are bound but the perturbations are different, or different amounts of  $\Delta$  and  $\Lambda$  are bound to DNA and the perturbations are different.

**Binding Affinity and Preferentiality.** The results in Table I and in Figure 10b (which also shows the preferentiality reported by Barton<sup>6</sup>) should be discussed together with the observed LD. All data consistently show that pure  $\Lambda$  has a high affinity for AT, and also binds well to DNA, even up to very high binding ratios ( $\approx 0.20$ ). By contrast,  $\Delta$  binds best to GC, though it also binds well to DNA at low binding ratios with the maximum binding ratio being somewhat lower ( $\approx 0.15$ ) for this enantiomer, as would be expected for an electrostatic-dependent binding. The more marked increase in preferentiality of  $\Lambda$  for AT (lower  $P$  value in Figure 10b) with higher binding ratios, compared to  $\Delta$  for GC, is consistent with a denser packing favoring  $\Lambda$  in the limit of saturated occupancy (see below). The racemate shows a markedly weaker apparent binding to DNA (and also to GC at high binding ratios) than either enantiomer. Recalling the effect of  $\Delta$  on the DNA orientation, a most plausible explanation is that the  $\Lambda$  binding is weakened by the structural perturbation of DNA caused by the simultaneous presence of the  $\Delta$  enantiomer. The effect is less pronounced with AT, as expected due to the weaker binding of  $\Delta$  to this polynucleotide. The LD spectra of racemate/DNA are also consistent with this conclusion, becoming more  $\Delta$ -like with higher binding ratios, despite the stronger binding to DNA of the pure  $\Lambda$  enantiomer when alone. The binding preferentiality (Figure 10b) for the polynucleotides/racemate is consistent with this.

**Binding Modes.** From steric and coulombic considerations, it seems clear that the metal complexes are groove binders. The rather similar affinities, similar degrees of spectral perturbation, and similar behavior with increasing salt concentration are consistent with both enantiomers being accommodated in a groove. The different binding behavior of the two enantiomers (LD evidencing different orientation and/or environments) might mean that one of the enantiomers binds to the minor groove and one to the major groove. Elongated groove binders, such as netropsin,<sup>31-34</sup> are known to bind selectively, mainly electrostatically, to AT-rich regions in the minor groove, and the stronger AT preference observed for the  $\Lambda$  complex might thus be due to minor-groove binding of this enantiomer. However, some indications make us believe that *both* enantiomers are to be exclusively

(31) Zimmer, C.; Reinert, K. E.; Luck, G.; Wähnert, U.; Löber, G.; Thrum, H. *Prog. Nucleic Acid Res. Mol. Biol.* **1971**, *15*, 285-318.

(32) Wartell, R. M.; Larson, J. E.; Wells, R. E. *J. Biol. Chem.* **1974**, *249*, 6719-6731.

(33) Kolchinskii, A. M.; Mirzabekov, A. D.; Zasedatelev, A. S.; Gurskii, G. V.; Grokhovskii, S. L.; Zhuze, A. L.; Gottikh, B. P. *Mol. Biol. (Moscow)* **1975**, *9*, 14-20.

(34) Patel, D. J. *Proc. Natl. Acad. Sci. U.S.A.* **1982**, *79*, 6424-6428.

(35) McCaffery, A. J.; Mason, S. F.; Norman, B. J. *J. Chem. Soc. A* **1969**, 1428-1441.

(36) Bosnich, B. *J. Am. Chem. Soc.* **1968**, *90*, 627-632.

(30) Schipper, P. E.; Nordén, B. *Chem. Phys.* **1981**, *57*, 365-376.



Table II. Spectroscopic Data for Determination of  $\kappa^a$ 

	$r$	LD	$S$	$I$	$[L]/\mu\text{M}$	$C_B/\mu\text{M}$	$\kappa$
DNA/ $\Delta$	0.021	-0.0048	0.064	0.078	$1.0 \pm 0.2$	$8.5 \pm 0.5$	0.36
	0.092	-0.0149	0.051	0.374	$14.1 \pm 1.0$	$34.7 \pm 2.5$	0.35
DNA/ $\Lambda$	0.047	-0.0030	0.149	0.158	$0.3 \pm 0.05$	$17.5 \pm 0.5$	0.64
	0.077	-0.0018	0.140	0.264	$0.9 \pm 0.1$	$30.3 \pm 1.5$	0.65

<sup>a</sup>LD( $A_2$ ) and  $I$ , referring to 480 nm in absorbance units and normalized to 1-cm path length;  $\kappa$  calculated according to eq 19 with  $\epsilon_F(480) = 6600 \text{ cm}^{-1} \text{ M}^{-1}$ .

found in the major groove. First, from model building it is clear that they fit well into the major groove but are too big to enter an unperturbed minor groove. Second, the relatively similar changes of the absorption spectra when the enantiomers bind to DNA suggest that the environments and average distances to the perturbing DNA chromophores are not extremely different. This seems inconsistent with, for example, the  $\Lambda$  complex being close to the phosphates at the mouth of the minor groove and the  $\Delta$  complex being buried in the major groove. Third, even if the  $\Lambda$  complex would prefer the minor groove, there is no reason why it should be excluded from binding in the major groove, which is in conflict with its isosbestic behavior with AT indicating only one binding site. Fourth, the increasingly more  $\Lambda$ -like LD spectra at high binding ratios of the racemate may indicate that  $\Delta$  and  $\Lambda$  compete for sites on AT; this is a weaker argument, though, since they may compete on electrostatic grounds also when in different grooves. We therefore propose that both enantiomers bind in the major groove of DNA, though with different geometries. The similar binding strengths of  $\Delta$  and  $\Lambda$  with DNA, and similar degrees of perturbation of normal absorption and CD spectra, support this.

It has been proposed that the  $\Delta$  enantiomer (and to a less extent  $\Lambda$  too) of  $[Ru(\text{phen})_3]^{2+}$  binds to DNA with one of the chelate wings intercalated between the base pairs.<sup>2-7,12,13</sup> The evidence that has been presented to support this hypothesis includes fluorescence quenching measurements,<sup>5,6</sup> unwinding studies,<sup>2,4</sup> luminescence measurements,<sup>4,5</sup> and changes in the normal absorption.<sup>4</sup> However, the differences between  $\Delta$  and  $\Lambda$  observed with each of these techniques are not large, and other explanations are feasible. For example, the observed "red shift" in the normal absorption is more likely to be due to different perturbations of the E and  $A_2$  CT bands than due to an actual red shift of the whole band. Also, the unwinding observed in circular DNA upon binding with metal complexes is similar for both enantiomers and is expected to occur when a large molecule binds in a DNA groove, intercalated or not. Our observations of decreased DNA orientation and the angular orientation of the complex (see below) and the higher affinity for AT of the  $\Lambda$  isomer are not in accord with this hypothesis. On the contrary, analysis of spectroscopic data suggests that  $\Lambda$  binds with one chelate parallel to the base pairs, while  $\Delta$  does not. This is in fact supported by the nonbinding<sup>6,13</sup> of the  $\Lambda$ - $[Ru(4,7\text{-diphenylphen})_3]^{2+}$ , which from molecular models is too bulky, having the substituent phenyl rings nonplanar with the phenanthroline, to bind in the manner apparently adopted by  $\Lambda$ - $[Ru(\text{phen})_3]^{2+}$  (see below). By contrast, the  $\Delta$ -diphenylphenanthroline complex does bind,<sup>6,13</sup> and the binding geometry of the unsubstituted  $\Delta$ -phenanthroline complex suggested below could accommodate the additional phenyl groups.

**Spectroscopic Analysis.** We here analyze the spectroscopic data summarized in Figures 2-8 more quantitatively, using the expressions given in the Theory section. To apply eqs 9-19, one requires a region of the spectrum that is due almost entirely to a transition of one polarization. This means the  $A_2$  band that lies on the low-energy side of the first CT band (see below for assignments) can be analyzed in some detail. Unfortunately, the high-energy side of the first CT band overlaps with a neighboring transition (cf. especially the CD spectrum of the free complex and also magnetic circular dichroism experiments<sup>37</sup>). Our analysis of the E band must therefore be less quantitative than that of the  $A_2$  band. The spectra in the region of 250 nm are harder to

analyze because both base and intraligand transitions occur there.

The similarity between free and bound spectra indicates that assignments appropriate for the free complex can be applied directly to the bound complex. The ZDO calculations of Mayoh and Day<sup>38</sup> indicate that the details of the assignments are far from straightforward.<sup>35</sup> However, for our purposes we need only the symmetry of a transition. Simple exciton arguments based on the ligand CD spectrum (250-nm region) indicate that the higher energy component of the ligand transition is the  $A_2$  band.<sup>35,36</sup> Since the  $A_2$  CT CD of an electric-dipole-allowed transition is opposite in sign from the  $A_2$  ligand CD,<sup>39</sup> the lower energy CT component can be assigned to be  $A_2$ . This assignment accords with the one suggested by the single crystal absorption measurements.<sup>40</sup>

Equations 9-18 all have the form of the product of an energy factor, the oscillator strength of the transition *in the absence* of DNA, and a term dependent on base-pair transition moments and the geometry of the system. Thus, for a given molecule the changes in each type of spectrum upon binding to DNA have approximately the same shape for all Z- (or X- or Y-) polarized transitions, and the magnitudes of the changes are determined mainly by the ratios of their transition moments, with a slight influence from the energy factor. It is therefore helpful to be able to also use the transitions in the 250-nm region, as the lower two bands have E polarization.

The metal complex LD in the 250-nm region can be determined by subtracting out the DNA LD. The LD<sub>metal</sub> spectra in this region resemble the corresponding CT LD spectra of the two enantiomers but with the  $A_2$  and E bands reversed. The CD in the 250-nm region is essentially due to the metal complex.

It is immediately apparent from the spectra that  $\Delta$  and  $\Lambda$  enantiomers interact differently with the DNA, so for clarity we shall consider each complex in turn, treating  $\Delta$  first. We begin our analysis with the CT  $A_2$  band at 480 nm. As the complexes have no LD in the absence of binding to the flow-oriented DNA, LD is the most sensitive probe of the metal complex/DNA interaction. As mentioned, it is helpful to subdivide the LD into two components, (i) LD<sup>0</sup>, which is the LD a complex would have when oriented by some means that does not involve any spectral perturbation of the complex, and (ii) LD', which results from the hyperchromic interactions of the complex with the DNA. LD<sup>0</sup> and LD' correspond to the different terms in each of eqs 12-14. Somewhat unexpectedly, LD' is the easier term to deal with, since it was shown to be  $(-3/2)\delta(I)$ .

This may be quantified by substituting the data from Table II into eq 19. From the resulting  $\kappa$  value, we can conclude that the 3-fold axis of the  $\Delta$  complex is oriented at an apparent angle of  $69 \pm 3^\circ$ . One conclusion to immediately be drawn from this is that Barton's proposed partially intercalated geometry is not appropriate for the  $\Delta$  complex (with one of the chelate rings parallel to the base plane, an angle of  $\cos^{-1}(1/\sqrt{3}) = 55^\circ$  would have been obtained).

It is often the case that preferred association geometries of two species are related to their symmetries. If we ignore asymmetry due to base sequence, a probable binding geometry for both complexes is then one where a 2-fold axis of the complex approximately aligns with the pseudo 2-fold rotation axis of DNA. This means that the X axis of the complex (which bisects a chelate) is approximately perpendicular to the z axis of DNA and parallel

(38) Mayoh, B.; Day, P. *Theor. Chim. Acta* 1978, 49, 259-275.

(39) Schipper, P. E.; Rodger, A. J. *Am. Chem. Soc.* 1983, 105, 4541-4550.

(40) Felix, F.; Ferguson, J.; Güdel, H. U.; Ludi, A. *Chem. Phys. Lett.* 1979, 62, 1, 153-157.

(37) Thomson, A. J.; Skarda, V.; Cook, M. J. *J. Chem. Soc., Dalton Trans.* 1985, 1781-1788.

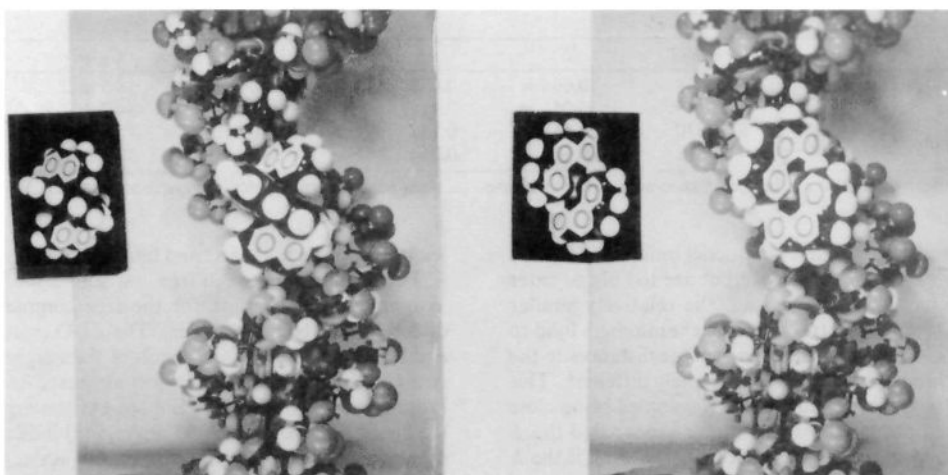


**Figure 11.** Proposed binding geometries of (left)  $\Delta$ - and (right)  $\Lambda$ -[Ru(phen)<sub>3</sub>]<sup>2+</sup> in the major groove of B-form DNA, viewed along a complex  $C_2$  axis. The aromatic rings of the phenanthroline chelates are indicated by white hexagons with dark circles.

to  $x$ , so  $\alpha \approx 1$  and  $\beta, \gamma, \delta,$  and  $\eta \approx 0$ ; as  $X, Y, Z$  is a right-handed system,  $\epsilon = \kappa$  and  $\zeta = -\theta$ . Two geometries of this symmetry are possible: one with one chelate along the major groove and the other with two chelates disposed in the groove. Equations 9–18 simplify considerably for this case. As LD is sensitive to the orientation of the complex with respect to the DNA axis and the CD depends on the orientation of the complex with respect to in-plane base-pair transition moments,<sup>41</sup> if a high-symmetry geometry is not adopted, some inconsistency in the LD or CD or absorption spectra for  $A_2$ - or E-polarized transitions should be apparent.

The normal absorption change of the CT  $A_2$  band is positive, so from eq 9, for a high-symmetry geometry, the  $tB_x B_y$  term must have the opposite sign from  $\theta$ . Thus the ratio  $\theta(R, A_2)/\delta(I, A_2)$  has the same sign as  $-\theta$ , so  $\delta(R, A_2)$  and  $-\theta$  have the same sign. This requires  $\theta > 0$  and the  $tB_x B_y$  term to be negative. Independent support for the sign of the  $tB_x B_y$  term comes from ref 41, which was a study of the CD of dyes intercalated into DNA. The results of ref 41 are in terms of a parameter that is negative and proportional to  $B_x^2 - B_y^2$  (using the notation of this work). Thus long-axis-polarized base-pair transition moments are, on average, larger than short-axis ones. The positions of the long and short axes of the base pairs, the twist of DNA, and the relative magnitudes of the moments then require that the  $tB_x B_y$  term is negative. So we conclude that  $\theta > 0$  for  $\Delta$ , and the  $Y$  axis of a  $\Delta$  complex is preferentially in the  $+z$  direction.

If the tris-chelate  $X/Y$  degeneracy is not split upon binding to DNA, then no additional geometric information results from analysis of the E band. However, the appearance of the LD spectrum for  $\Delta$ , with a sign change within the "E band", indicates the  $X/Y$  degeneracy is lifted so we must consider two E transitions. As  $\mu(X)^2 = \mu(Y)^2$  for unperturbed  $\Delta$ , in the proposed high-symmetry binding mode  $LD^0(X)$  is required to be negative and  $LD^0(Y)$  to be positive and approximately twice the magnitude of  $LD^0(X)$ . From eqs 10 and 11,  $LD'(X) = (-3/2)\delta(I, X) < 0$ , an  $LD'(Y) = (-3/2)\delta(I, Y) > 0$  and again larger than  $LD'(X)$ . This is consistent with the CT LD E band if we assign the  $X$ -polarized component to be lower in energy than the  $Y$ -polarized component. In addition,  $\delta(R, X)$  is expected to be positive, which is consistent with the observed perturbed CD spectrum that at low energy ( $A_2$  region) is more negative than the unperturbed spectrum but is more positive in the  $X$  region and less positive in the  $Y$  region.

Thus for  $\Delta$ , the  $A_2$  LD spectrum shows the angle made by the 3-fold axis with the DNA axis to be  $69 \pm 3^\circ$ , and the CD and normal absorption of the  $A_2$  transition and the LD, CD, and normal absorption of the E transition are all consistent with a high-symmetry binding geometry where two chelates fit into the

major groove (required by  $\theta > 0$ ). This geometry is illustrated in Figure 11.

We now turn to  $\Lambda$ , following much the same analysis used for the  $\Delta$  complex, although the situation is not quite as clear-cut. From the observation that the  $A_2$  LD band is much less negative for  $\Lambda$  than for  $\Delta$  (this is even more so than indicated by the spectra in Figure 2, as the  $S$  factor for  $\Lambda$  is about 2 times as large as that for  $\Delta$ ), we conclude that  $\kappa(\Lambda)^2$  is significantly greater than  $\kappa(\Delta)^2$ . Application of eq 19 enables us to quantify this: the 3-fold axis of the  $\Lambda$  complex is oriented at an apparent angle of  $50 \pm 2^\circ$  relative to the DNA axis. As noted above, this orientation is consistent with one of the chelate wings being approximately parallel to the base pairs.

Let us now determine whether a high-symmetry geometry is also appropriate for  $\Lambda$ . As for  $\Delta$ , the  $tB_x B_y$  term has the same sign as  $-\theta$ . So from ref 41 we would again expect  $\theta > 0$ , which requires  $\delta(R, A_2) < 0$ . It is not clear from the CD spectra that this is in fact the case. Equations 17 and 18 lead us to expect a large positive value for  $\delta(R, E)$  for  $\Lambda$  as  $\kappa$  is large, and the small experimental  $\delta(R, A_2)$  at the low-energy side of the CT spectrum supports a negative  $\delta(R, A_2)$ . The high-energy ( $A_2$ ) side of the intraligand transition also provides tenuous support for  $\delta(R, A_2) < 0$ .

$LD^0(X)$  for  $\Lambda$  is the same as for  $\Delta$ , and  $LD^0(Y)$  for  $\Lambda$  is approximately equal to  $-LD^0(X)$ .  $LD'(X)$  is also the same for both complexes in high-symmetry geometries. However,  $LD'(Y)$  is significantly larger for  $\Lambda$  than for  $\Delta$  (up to 8 times as large), resulting in a net positive LD(E) signal. The  $X/Y$  degeneracy is more nearly retained for  $\Lambda$  than for  $\Delta$ , though the same  $X, Y$  assignment can tentatively be made. Thus a high-symmetry binding geometry, with a chelate approximately parallel to the DNA base pairs, is consistent with the observed CD spectra of the  $\Lambda$  enantiomer, where  $\delta(R, A_2)$  is in fact negative.

**Binding Geometries.** Thus a very simple explanation of the observed two types of binding characteristics has emerged, namely, that they correspond to the two possible ways of accommodating a  $D_3$  complex with the 2-fold axis oriented preferentially approximately perpendicular to the DNA helix axis: either one or two of the chelate wings are symmetrically facing the groove. From analysis of  $A_{iso}$ , LD, and CD spectra, we propose that the  $\Lambda$  enantiomer has a single chelate pointing in toward the DNA, lying parallel to the DNA base pairs. This proposed geometry is consistent with other experimental data: (i) The two outer chelates will tend to bridge phosphates of opposite strands, resulting in a more rigid DNA structure that is consistent with the high orientation parameter for  $\Lambda$ . (ii) The average orientation of the inner single chelate phenanthroline, approximately coplanar with a base pair, will make this geometry more sensitive to base sequence, in accordance with the absence of an isosbestic point in the LD spectra of  $\Lambda$ /DNA. (iii) This geometry allows economical

(41) Schipper, P. E.; Nordén, B.; Tjernereld, F. *Chem. Phys. Lett.* **1980**, *70*, 17–21.

packing of up to six complexes per DNA turn (binding ratio = 0.3), in agreement with the observed high maximum occupancy of the  $\Lambda$  enantiomer. (iv) This efficient packing of  $\Lambda$  explains the retained high binding affinity of this enantiomer to DNA at high binding ratios and the markedly decreased affinity of the racemate in the presence of  $\Delta$  that does not costack with  $\Lambda$ . (v) The amino groups pointing into the major groove of  $[\text{poly}(\text{dG-dC})]_2$  are not expected to interact favorably with the single chelate wing in the proposed geometry for the  $\Lambda$  complex; their absence in  $[\text{poly}(\text{dA-dT})]_2$ , where the hydrophobic thymine methyl pointing into the major groove and the more negative thymine oxygen and aza lone pair of adenine could be anticipated to favor binding to the latter polynucleotide, is in accord with the observed high binding affinity of  $\Lambda$  for  $[\text{poly}(\text{dA-dT})]_2$ .

Correspondingly, we have proposed a preferred geometry for the  $\Delta$  enantiomer with two chelate wings pointing in toward the DNA and again the 2-fold axis being perpendicular to the DNA helix. Some supporting arguments are as follows: (i) The two chelate wings fit facing into the helical stack of bases and the orientation of the complex is thereby firmly defined in agreement with the fluorescence polarization anisotropy,<sup>5,6</sup> which indicates a more rigid binding than for the  $\Lambda$  complex. (ii) The complex orientation is determined only by the average pitch of the helix, in agreement with its isosbestic behavior even in heterogeneous DNA. (iii) The presence of the two chelates inside the groove is consistent with a perturbed DNA structure and lower orientation factor. (iv) Close approach of the chelates inside the groove makes binding of more than three complexes per DNA turn (binding ratio 0.15) energetically unfavorable, in agreement with the lower maximum occupancy observed for  $\Delta$ . (v) In  $[\text{poly}(\text{dG-dC})]_2$ , the major-groove guanine amino group that is closest to the complex will, in the proposed geometry, fit in between the two chelates and be in proximity to the ruthenium, which may stabilize the binding of the  $\Delta$  enantiomer and potentially destabilize the base pairing.

## Conclusions

Systematic studies have been performed on the interactions between DNA, as well as polynucleotides, and the  $\Delta$  and  $\Lambda$  enantiomers of  $[\text{Ru}(\text{phen})_3]^{2+}$  (including the racemate). The work of this paper illustrates well the utility of flow LD for studying DNA interactions. The main reason for this is that only bound species are probed. The normal absorption and circular dichroism spectroscopic methods complement this technique, enabling binding geometries to be deduced. There are a number of important conclusions to be made from this study.

(1)  $\Delta$  and  $\Lambda$  enantiomers both bind to DNA but with different geometries, binding strengths, and spectral perturbations.

(2) For each enantiomer, the geometry (and perturbation) is essentially independent of base-pair composition.

(3) By contrast, the binding affinity (and preferentiality) varies with base-pair composition, binding ratio, and ionic strength.

(4) There is a competition between  $\Lambda$  and  $\Delta$ , but each enantiomer has its own binding geometry.

(5)  $\Delta$  and  $\Lambda$  affect the flow orientation of DNA differently. At small binding ratios  $\Delta$  causes a sharp decrease in orientation, whereas  $\Lambda$  causes a slight increase followed by a decrease when the binding ratio is increased.

(6) Nondegenerate exciton perturbation from the DNA bases markedly changes the LD intensities and has to be corrected for when LD is used analytically to determine geometries. The changes in dipole strength observed for normal absorption are utilized for this purpose.

(7) The LD data are consistent with an arrangement of the  $\Delta$  complex in which the 3-fold axis makes an angle of approximately 70° with the DNA axis. A corresponding angle of 50° is obtained for the  $\Lambda$  complex. Further information about the binding geometries is extracted from the CD and normal absorption data. The spectra were found to be consistent with the lifting of the E degeneracy upon perturbation by DNA.

It is most likely that both  $\Delta$  and  $\Lambda$  bind in the major groove of DNA and that the steric interactions between the chelate wings

of the metal complex and the sides of the groove lead to different geometries.

On the bases of symmetry and spectral analysis we have proposed two types of binding geometries, both characterized by having the 2-fold axis of the complex parallel to the DNA dyad axis. For the  $\Lambda$  complex, we suggest a geometry where one chelate wing points into the middle of the major groove and in which the stability and average orientation are mainly determined by interaction of the two remaining wings with phosphates of the strands. For the  $\Delta$  complex, we propose the "opposite" geometry where two chelates sit in the groove and determine the orientation by closely fitting the helical stack of base pairs.

The well-defined characteristic binding geometries, apparently insensitive to base composition, binding density, ionic strength, and presence of the opposite enantiomer, are in contrast to binding affinities that sensitively depend on these conditions. One may thus speculate whether a precisely defined orientation of a nucleic acid adduct is required for biological recognition, just as a lock is opened most easily when the correct key in the correct orientation is inserted.

**Acknowledgment.** Support from the Swedish Natural Science Research Council is gratefully acknowledged.

## Appendix

The normal absorption ( $A_{\text{iso}}$ ) and circular dichroism (CD) spectra of  $[\text{Ru}(\text{phen})_3]^{2+}$  in the presence of DNA are sufficiently like the corresponding spectra of the free complex for the effect of the DNA to be treated as a perturbation. If the geometry of the complex is not altered by its interaction with DNA, then the perturbation can be expressed by using perturbation theory and an electrostatic interaction of the complex with the DNA.

The transitions of interest in the metal complex are the first electric-dipole-allowed (eda) charge-transfer (CT) transitions and the first intraligand (IL) transitions. The three spectroscopic phenomena for which we require theoretical expressions to aid analysis of the experimental data are (1) changes in  $A_{\text{iso}}$  intensity upon interaction with DNA, denoted  $\delta(I)$ , (2) the linear dichroism resulting from orientation and interaction with DNA, denoted LD, and (3) changes in CD upon interaction with DNA, denoted  $\delta(R)$ .

We assume that the effect of any geometry change is at most to lift the  $X/Y$  degeneracy in the complex. The interaction of the DNA with a complex transition is expressed in terms of an electrostatic coupling,  $V$ , of the DNA and the complex, and perturbation theory is used to determine the effect of the interaction on the spectroscopic properties of the complex. With a sufficiently large separation between the complex origin and the origins of DNA chromophores, the multipolar expansion of  $V$  can be truncated at dipolar terms, since successive terms have higher inverse  $r$  dependences.

$$V = \mu_a \cdot \rho C^0 / r^2 + (\mu_a \cdot \mu_b - 3\mu_a \cdot \rho \mu_b \cdot \rho) / r^3 \quad (\text{A1})$$

where  $C^0$  is the charge of a DNA chromophore (since the DNA charge is largely localized to the phosphate backbone,  $C^0 = 0$ ),  $\mu_a$  and  $\mu_b$  are the electric dipole transition moment operators of the complex and of a chromophore of DNA,  $\rho$  is the unit vector along a line connecting the complex origin to that of a DNA chromophore, and  $r$  is the distance between those origins. Summation over DNA chromophores is implied.

Assuming real wave functions, the perturbed forms of the ground and excited states of a transition on the complex may be expressed to first order in the perturbation as

$$|o\rangle = |oo\rangle - \sum_{ab} \frac{\langle ab|V|oo\rangle}{(\epsilon_a + \epsilon_b)} |ab\rangle \quad (\text{A2})$$

$$|e\rangle = |1o\rangle - \sum_{ab} \frac{\langle ab|V|1o\rangle}{(\epsilon_a + \epsilon_b - \epsilon_1)} |ab\rangle \quad (\text{A3})$$

where  $|ab\rangle$  denotes the product basis function  $|a\rangle|b\rangle$  in which  $|a\rangle$  is a wave function of the isolated complex that has transition energy  $\epsilon_a$  from the ground state  $|1o\rangle$  and  $|b\rangle$  is a wave function

of a DNA chromophore (usually a base pair) at transition energy  $\epsilon_b$  from the ground state;  $\epsilon_1$  is the transition energy of the transition of interest; and summation over all chromophores of the DNA is implied. The electric dipole transition moment of the  $|o\rangle \rightarrow |e\rangle$  transition is then

$$\mu(|o\rangle \rightarrow |e\rangle) = \mu_a^{01} - \frac{\mu_a^{0a} \rho C^0 \mu_a^{a1}}{\epsilon_a r^2} - \frac{\mu_a^{a1} \rho C^0 \mu_a^{0a}}{(\epsilon_a - \epsilon_1) r^2} - \frac{\mu_a^{01} \mu_b^{b0} - 3\mu_a^{01} \rho \rho \mu_b^{b0}}{(\epsilon_b - \epsilon_1) r^3} \mu_b^{0b} - \frac{\mu_a^{01} \mu_b^{0b} - 3\mu_a^{01} \rho \rho \mu_b^{0b}}{(\epsilon_b + \epsilon_1) r^3} \mu_b^{b0} - \frac{\mu_a^{0a} \mu_b^{00} - 3\mu_a^{0a} \rho \rho \mu_b^{00}}{\epsilon_a r^3} \mu_a^{a1} - \frac{\mu_a^{a1} \mu_b^{00} - 3\mu_a^{a1} \rho \rho \mu_b^{00}}{(\epsilon_a - \epsilon_1) r^3} \mu_a^{0a} \quad (\text{A4})$$

where  $\mu = \mu_a + \mu_b$ , summation over  $|a\rangle$  and  $|b\rangle$  and DNA chromophores is implied, and the superscripts on the transition moments denote the states they connect. For an  $A_2(Z)$ -polarized transition on the complex, the terms dependent on  $C^0$  vanish for symmetry reasons and because  $C^0 = 0$ . As our analysis is based on the  $A_2$  band, we shall henceforth omit explicit reference to the DNA charge-dependent terms. In addition, the terms dependent on permanent moments are usually smaller than those dependent on transition moments.

The perturbed magnetic dipole transition moment of  $|e\rangle \rightarrow |o\rangle$  is then approximately

$$\mathbf{m}(|e\rangle \rightarrow |o\rangle) = \mathbf{m}_a^{10} - \frac{\mu_a^{10} \mu_b^{0b} - 3\mu_a^{10} \rho \rho \mu_b^{0b}}{(\epsilon_b - \epsilon_1) r^3} [\mathbf{m}_b^{b0} + ir(\rho \times \mu_b^{b0}) \epsilon_b 2\pi / h] - \frac{\mu_a^{10} \mu_b^{b0} - 3\mu_a^{10} \rho \rho \mu_b^{b0}}{(\epsilon_b + \epsilon_1) r^3} [\mathbf{m}_b^{0b} - ir(\rho \times \mu_b^{0b}) \epsilon_b 2\pi / h] \quad (\text{A5})$$

where  $i = (-1)^{1/2}$  and  $\mathbf{m}_a$  and  $\mathbf{m}_b$  are the intrinsic magnetic transition moment operators of the complex and DNA base, respectively. The additional term, compared with the electric dipole transition moment, results from including the magnetic dipole with respect to the complex origin, which is due to the linear motion of electron density in a base pair. (It should be noted that there is no charge analogue of this term, since the charge term involves only electric dipolar transition moments on the complex that have no magnetic component about the complex origin).

Equation A5 has been expressed by using the equivalence of the velocity- and position-dependent formalisms in terms of electric dipole transition moments. The electric dipole term dominates the contribution from the intrinsic magnetic transition moments [due to (i) its smaller inverse distance dependence ( $r^{-2}$  compared with  $r^{-3}$ ) and (ii) the small size of magnetic transition moments compared with electric transition moments], so we shall concentrate on it. Using real wave functions, we can then write

$$\mathbf{m}(|e\rangle \rightarrow |o\rangle) = \mathbf{m}_a^{10} - i \frac{\epsilon_1 \epsilon_b 4\pi}{h(\epsilon_b^2 - \epsilon_1^2) r^2} (\mu_a^{10} \mu_b^{b0} - 3\mu_a^{10} \rho \rho \mu_b^{b0}) \rho \times \mu_b^{b0} \quad (\text{A6})$$

The dominant contribution to the spectroscopic properties we require can be directly determined from eqs A4 and A6 by using real wave functions, to be

$$\delta(I) = \mu(|o\rangle \rightarrow |e\rangle) \cdot \mu(|e\rangle \rightarrow |o\rangle) - \mu_a^{01} \mu_a^{10} - \frac{4\epsilon_b \mu_a^{01} \mu_b^{0b}}{(\epsilon_b^2 - \epsilon_1^2) r^3} (\mu_a^{01} \mu_b^{b0} - 3\mu_a^{01} \rho \rho \mu_b^{b0}) \quad (\text{A7})$$

$$\text{LD} = [\mu(|o\rangle \rightarrow |e\rangle)_z]^2 - \frac{1}{2} [\mu(|o\rangle \rightarrow |e\rangle)_x]^2 + [\mu(|o\rangle \rightarrow |e\rangle)_y]^2 = [\mu_a^{01} z]^2 - \frac{1}{2} [\mu_a^{01} x]^2 + [\mu_a^{01} y]^2 - \frac{4\epsilon_b}{(\epsilon_b^2 - \epsilon_1^2) r^3} (\mu_a^{01} \mu_b^{b0} - 3\mu_a^{01} \rho \rho \mu_b^{b0}) \{ \mu_a^{01} z \mu_b^{0b} z - \frac{1}{2} [\mu_a^{01} x \mu_b^{0b} x + \mu_a^{01} y \mu_b^{0b} y] \} \quad (\text{A8})$$

where  $x$ ,  $y$ , and  $z$  subscripts denote the  $x$ ,  $y$ , and  $z$  components of vectors,  $z$  being the direction of orientation of the complex.

$$\delta(R) = \text{Im} [\mu(|o\rangle \rightarrow |e\rangle) \cdot \mathbf{m}(|e\rangle \rightarrow |o\rangle) - \mu_a^{01} \mathbf{m}_a^{10}] = - \frac{\epsilon_1 \epsilon_b 4\pi}{h(\epsilon_b^2 - \epsilon_1^2) r^2} (\mu_a^{01} \mu_b^{b0} - 3\mu_a^{01} \rho \rho \mu_b^{b0}) \mu_a^{01} \rho \times \mu_b^{b0} \quad (\text{A9})$$

Equations 9–18 in the main text follow directly from eqs A7–A9 if DNA is represented only by transition moments that are perpendicular to the DNA axis, i.e., if  $\mu_b^{b0}$  has no  $z$  component (the intense  $\pi^* \leftarrow \pi$  transitions of the DNA bases are by symmetry polarized in the molecular plane, i.e., essentially  $xy$  polarized<sup>26</sup>).

**Registry No.** [Ru<sup>II</sup>(1,10-phenanthroline)<sub>3</sub>]<sup>2+</sup>, 22873-66-1; poly(dA-DT), 26966-61-0; poly(dG-dC), 36786-90-0.